ARMY RESEARCH LABORATORY

Modeling of Light Airborne High-frequency (HF) Antennas

by Christopher S. Kenyon

ARL-TR-5837 December 2011

NOTICES

Disclaimers

The findings in this report are not to be construed as an official Department of the Army position unless so designated by other authorized documents.

Citation of manufacturer's or trade names does not constitute an official endorsement or approval of the use thereof.

Destroy this report when it is no longer needed. Do not return it to the originator.

Army Research Laboratory
Adelphi, MD 20783-1197

ARL-TR-5837 **December 2011**

Modeling of Light Airborne High-frequency (HF) Antennas

Christopher S. Kenyon
Sensors and Electron Devices Directorate, ARL

REPORT DOCUMENTATION PAGE	Form Approved OMB No. 0704-0188

1. REPORT DATE *(DD-MM-YYYY)*	2. REPORT TYPE	3. DATES COVERED (From - To)
December 2011	Final	

4. TITLE AND SUBTITLE	5a. CONTRACT NUMBER
Modeling of Light Airborne High-frequency (HF) Antennas	5b. GRANT NUMBER
	5c. PROGRAM ELEMENT NUMBER

6. AUTHOR(S)	5d. PROJECT NUMBER
Christopher S. Kenyon	5e. TASK NUMBER
	5f. WORK UNIT NUMBER

7. PERFORMING ORGANIZATION NAME(S) AND ADDRESS(ES)	8. PERFORMING ORGANIZATION REPORT NUMBER
U.S. Army Research Laboratory ATTN: RDRL-SER-U 2800 Powder Mill Road Adelphi MD 20783-1197	ARL-TR-5837

9. SPONSORING/MONITORING AGENCY NAME(S) AND ADDRESS(ES)	10. SPONSOR/MONITOR'S ACRONYM(S)
	11. SPONSOR/MONITOR'S REPORT NUMBER(S)

12. DISTRIBUTION/AVAILABILITY STATEMENT

Approved for public release; distribution unlimited.

13. SUPPLEMENTARY NOTES

14. ABSTRACT

Performance of three lightweight, high-frequency (HF), airborne antenna designs are compared using FEKO method-of-moments modeling software. Of interest were the beam patterns near the ground. All three are upside down with ¼-wave counterpoise wires at the top. The antennas are fed between the base and the counterpoises. Two are ¼-wave monopole antennas while a third is a combination of cross-connected half and ¼-wave coaxial lines. Field strengths reaching the ground at a distance of up to 10 km, with the antennas suspended about four wavelengths above a uniform real ground, were computed.

15. SUBJECT TERMS

HF antennas, monopole antennas, light weight antennas for HF

16. SECURITY CLASSIFICATION OF:			17. LIMITATION OF ABSTRACT	18. NUMBER OF PAGES	19a. NAME OF RESPONSIBLE PERSON
a. REPORT	b. ABSTRACT	c. THIS PAGE			Christopher S. Kenyon
Unclassified	Unclassified	Unclassified	UU	28	19b. TELEPHONE NUMBER (*Include area code*) (301) 394-5547

Standard Form 298 (Rev. 8/98)
Prescribed by ANSI Std. Z39.18

Contents

List of Figures

Acknowledgments

I would like to thank Chris Fazi for proposing this study, as well as for his discussions of the three basic antenna designs, and Marc Ressler for discussions and suggestions concerning basic antenna properties.

INTENTIONALLY LEFT BLANK.

1. Introduction

In this study, we examine the beam patterns of three lightweight antenna designs from three different antenna models that are suspended about four wavelengths (λ) above a real ground plane. We used FEKO software with the method of moments (MOM) to compute the electrical characteristics of the proposed models such as currents, impedances, and fields. Of particular interest are the ground-pointed beam patterns at a distance of about 10 km from the antenna location. Other parameters of interest include the antenna impedance and its light weight. We seek a lightweight (<10 kg) antenna that can deliver the most energy out to that distance. Since the frequencies of interest are in the high-frequency (HF) band, the antenna is large (30-m wavelength).

2. Antenna Designs

We consider three antenna model designs. Two are simple upside-down, ¼ wave dipole antennas connected to a horizontal counterpoise or grounding wire (the L and T antennas) and the third is also a linear antenna connected to a counterpoise wire at its top (the segmented coaxial antenna). Unlike the first two, which consist of only wires, the third is largely a combination of coaxial lines. The models are idealized and do not include support structures and are fed with ideal power sources.

2.1 Inverted "L" antenna

Figure 1 shows the dimensions of the L antenna and the currents on it at resonance calculated by FEKO software using a MOM calculation. The ground wire is orthogonal to the vertical ¼-wave antenna. The FEKO model predicts a 41-Ω impedance, which is not too far off from the theoretical 37-Ω value for a vertical monopole antenna.

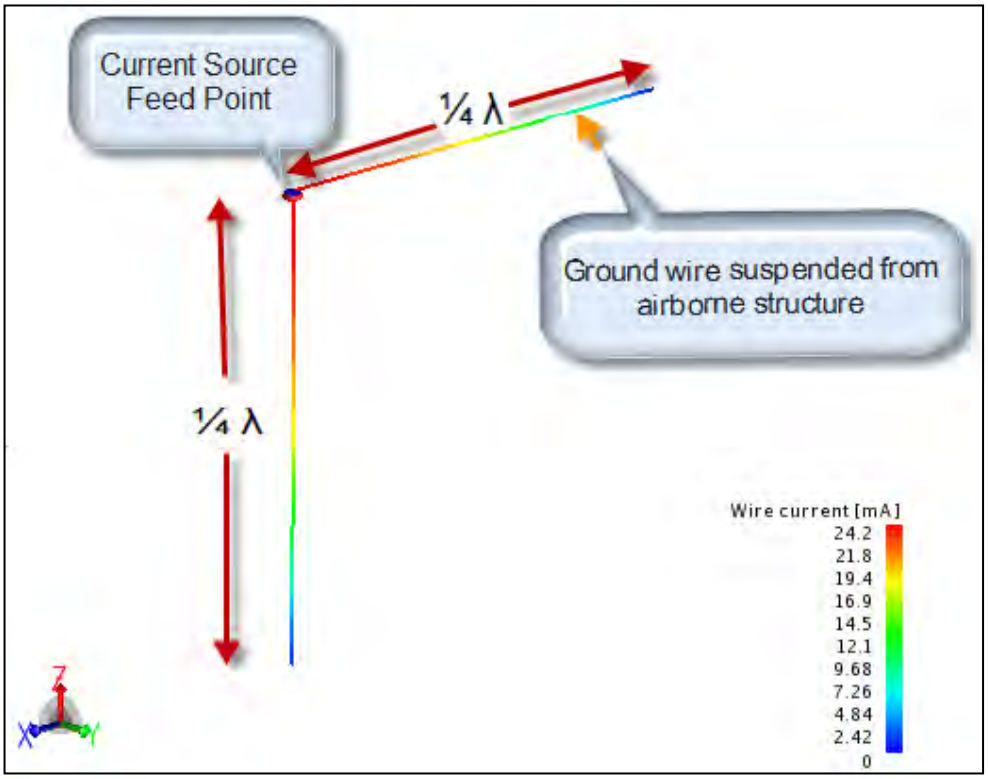

Figure 1. Inverted L antenna showing dimensions in wavelengths and computed current distribution.

2.2 "T" Antenna

Figure 2 shows the dimensions of the T antenna and the currents on it at resonance calculated by FEKO software using a MOM calculation. It differs from the L antenna by adding another ¼-wave wire to the ground, doubling its length as seen in the figure. Its computed impedance at resonance is 23 Ω, much lower than the 37-Ω monopole antenna impedance, but still high enough to be matched to 50 Ω by use of a 2:1 balun.

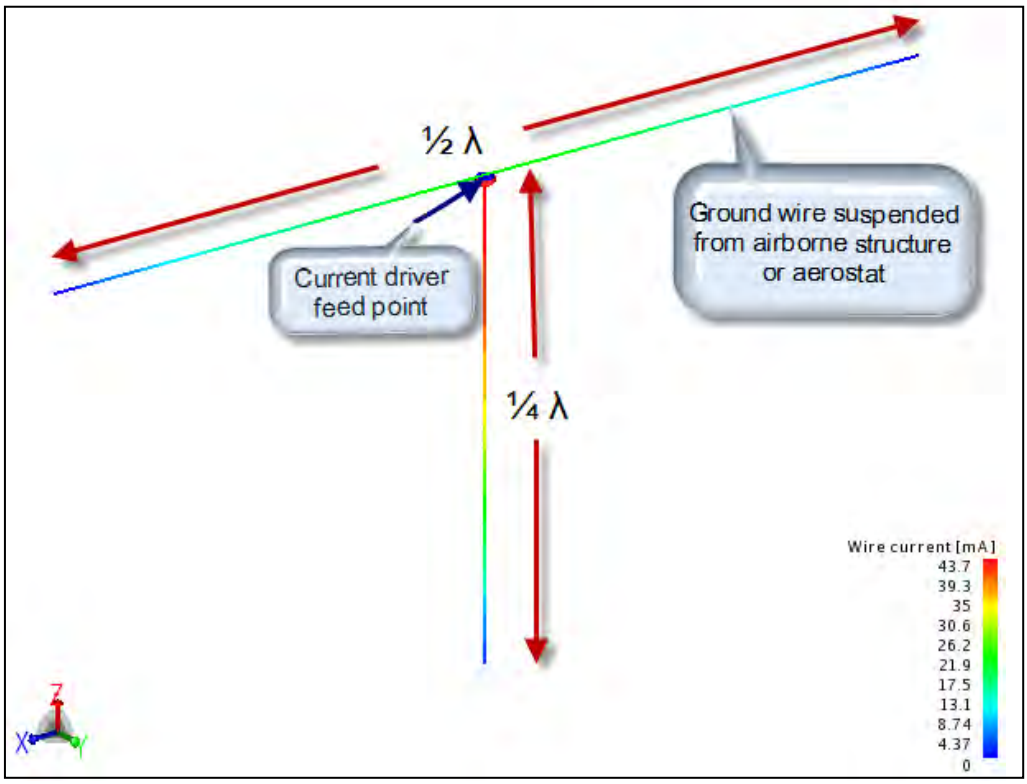

Figure 2. T antenna showing dimensions in wavelengths and current distribution.

2.3 A segmented coaxial antenna

Figure 3 shows a schematic of a segmented antenna, where the vertical ¼-wave wire of the T antenna is replaced by a series of coaxial sections with alternating connections. Its computed input impedance is 87 Ω, considerably off from the 37 Ω of a monopole antenna, due to the complex impedance transformation of the various coax lines. The figure shows the coax line greatly widened to illuminate the connections between the sections. While a physical coax would have a dielectric ($\varepsilon_r > 1$) to allow a small coax radius, we modeled it without any so that the radius would have to be larger for the same characteristic impedance.

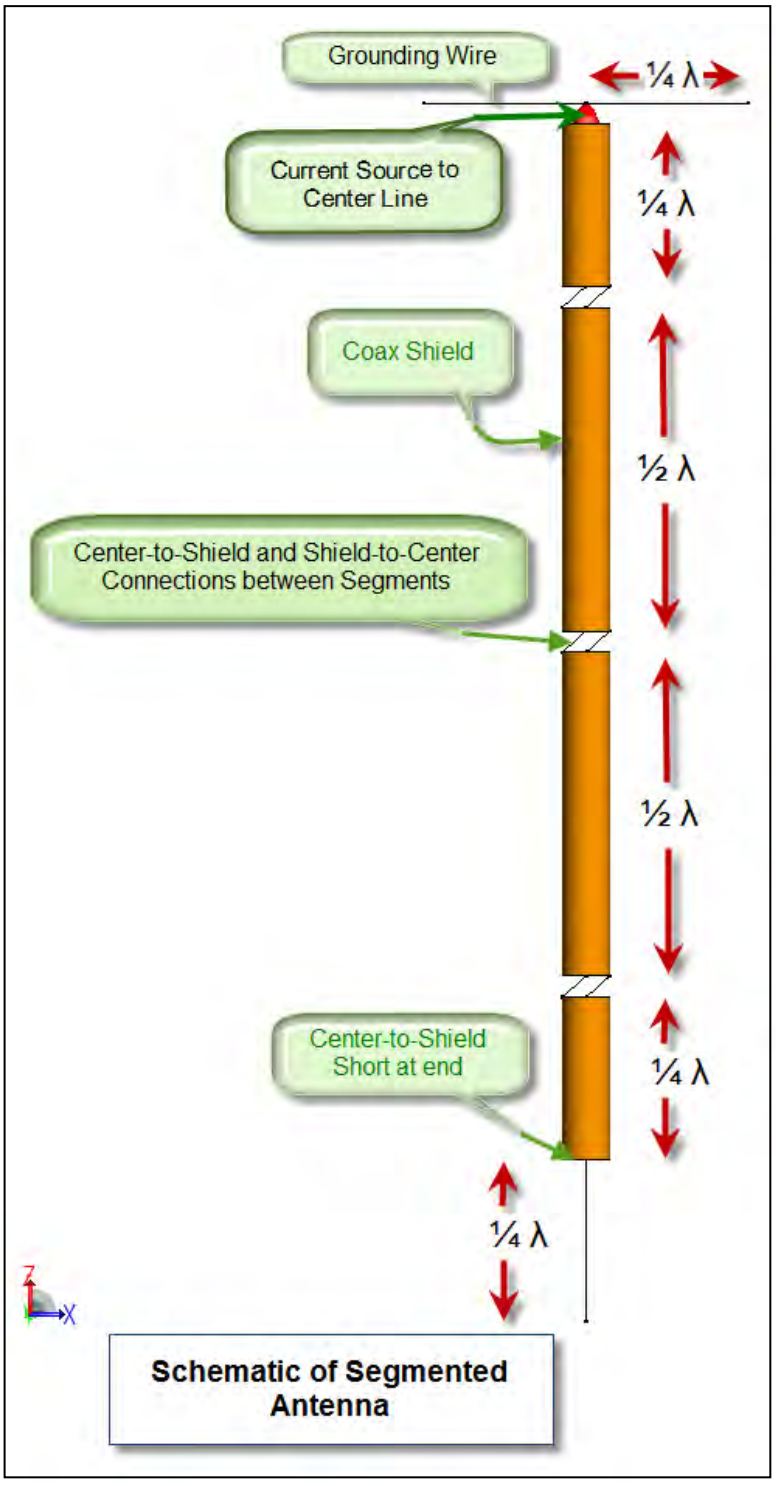

Figure 3. Schematic of segmented coaxial antenna with dimensions.

The actual modeling of the coax sections also used much larger coax shield and inner conductor radii in order to both render the size of the computation manageable while retaining a shield to inner conductor ratio consistent with an impedance of 50 Ω for the coaxial line. Larger radii in

the modeling allow for fewer triangles to represent the surfaces since the triangles are required* to have modest aspect ratios. From Pozar[1], we have the impedance of a coaxial line of $Z_0 = \frac{1}{2\pi}\sqrt{\frac{\mu}{\varepsilon}}\, ln\left(\frac{b}{a}\right)$, where a is the center conductor radius and b is the inside radius of the outer conductor. Since no dielectric is modeled, we have $\sqrt{\frac{\mu}{\varepsilon}} = 377\ \Omega$, where μ and ε are the permeability and permittivity of free space, respectively. Accordingly, in order to create a coaxial line with a characteristic impedance $Z_0 = 50\ \Omega$, we must set the ratio $\frac{b}{a} = exp\left(\frac{2\pi\ 50}{377}\right) = 2.3$. Figure 4 shows the current distribution on segmented antenna computed by FEKO.

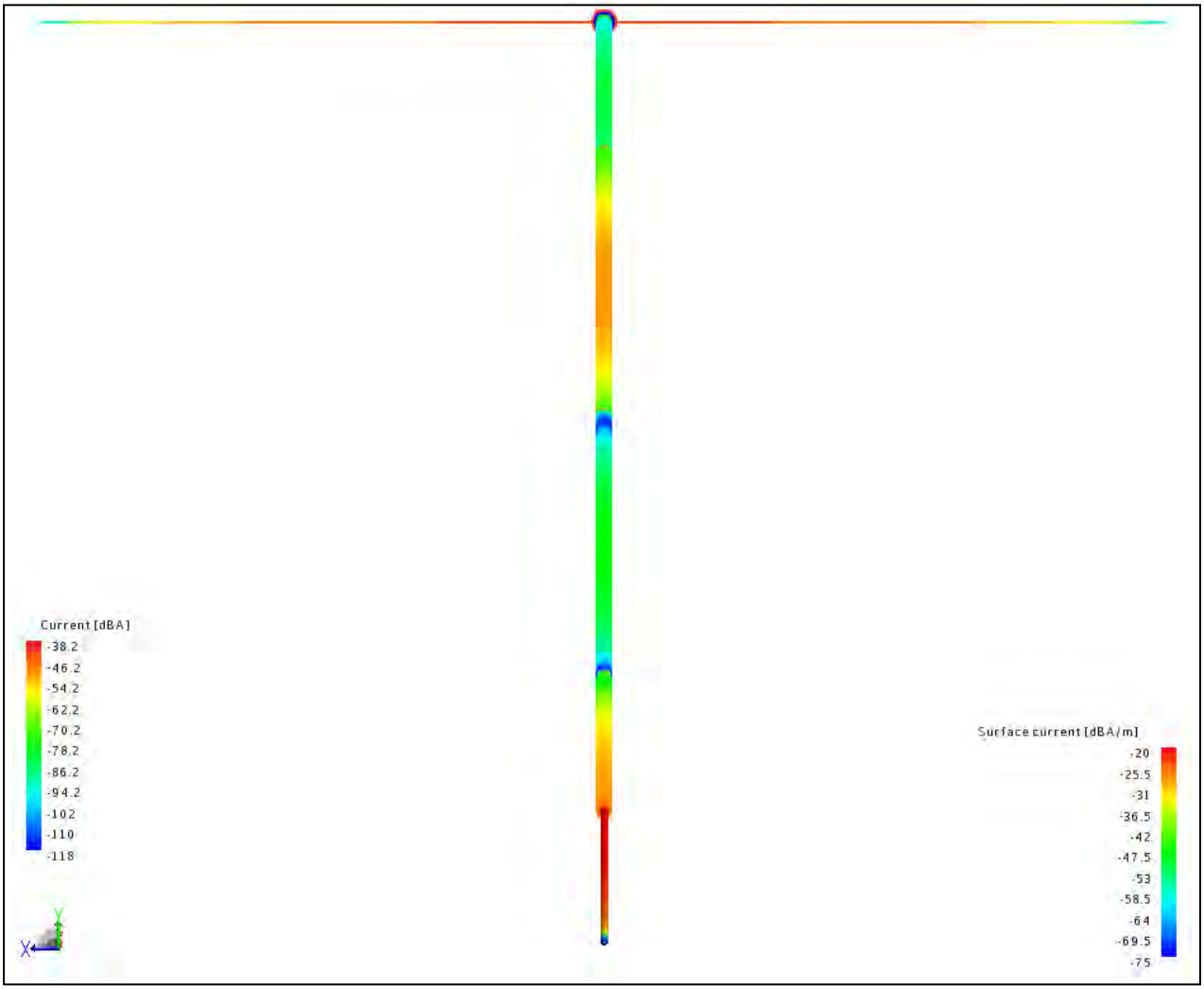

Figure 4. Current distribution on segmented antenna computed by FEKO.

* This requirement has been relaxed via anisotropic meshing in the more recent FEKO 6.1 version (FEKO 6.1 seminar, August 29, 2011).

[1] Pozar, D. M. *Microwave Engineering*, Addison-Wesley, 1990.

3. Fields

Using FEKO, I computed field distributions from the computer models or facet files of the antennas both in free space and over a flat real ground. The modeling assumed perfect conductors so that directivity and gain are the same. The L and T antennas showed typical donut-shaped field distributions in free space as in figure 5, while the segmented antenna had more lobes with a strong downward one as shown in figure 6. In these FEKO plots, the antennas, neglecting the counterpoises, are aligned along the *z*-axis while the counterpoises are parallel to the *x*-axis. The θ angle is from the *z*-axis so that ground is at θ = 90°.

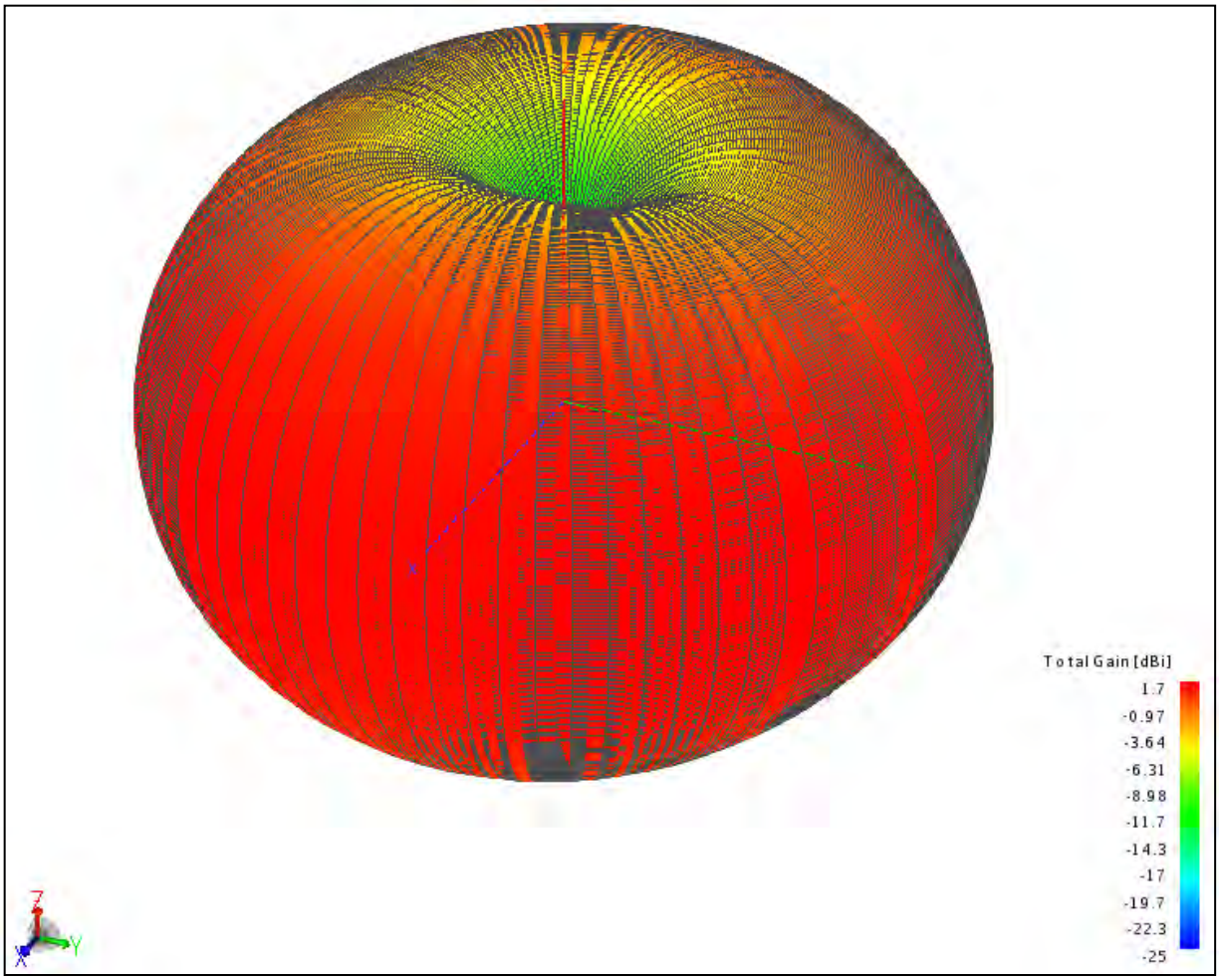

Figure 5. Gain pattern for T antenna in free space.

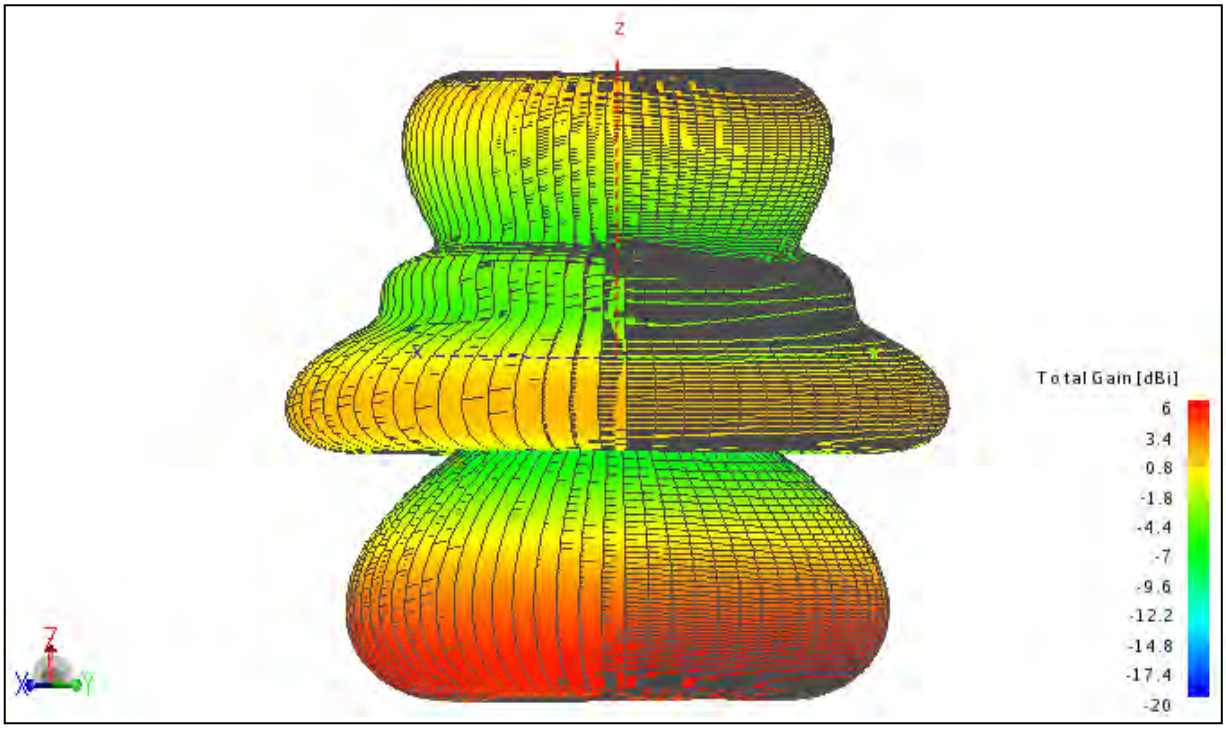

Figure 6 Gain pattern for multi-coax segmented antenna in free space.

3.1 Far Fields Over a Real Ground

Ground reflected fields combined with direct fields from the antenna result in an interference pattern that determines the field received at a distance. The ground conductivity, σ, and its relative dielectric constant, ε_r, determine the strength of the reflected field. In this study, σ was set to 0.005 S and ε_r was set to 10 to represent a uniform and typically moist soil.

Figures 7 through 12 depict the computed gain (or directivity) for all three antennas. The gains or field patterns are quite different from those in free space because of the ground reflected interference. For an observer or target increasing in elevation, the paths of the direct and reflected waves increasingly diverge. The phase difference between the two paths results in alternate constructive and destructive interference with increasing target elevation. Figures 8, 10, and 12 show the resultant interference versus θ. Similarly, if the elevation of the antenna is changed, as in figure 13, this also changes the phase difference between the two paths. In particular, increasing the antenna elevation causes a more rapid change in phase differences in θ, resulting in a denser lobe pattern. All three antennas have all a sizeable lobe near the ground. However, two of the antennas show more energy delivered into unfavorable directions, either up or down, indicating less energy available near the ground. Specifically the L antenna has more of its energy going up and nearly straight down than the T antenna. The segmented antenna had even more of its energy going up and nearly straight down.

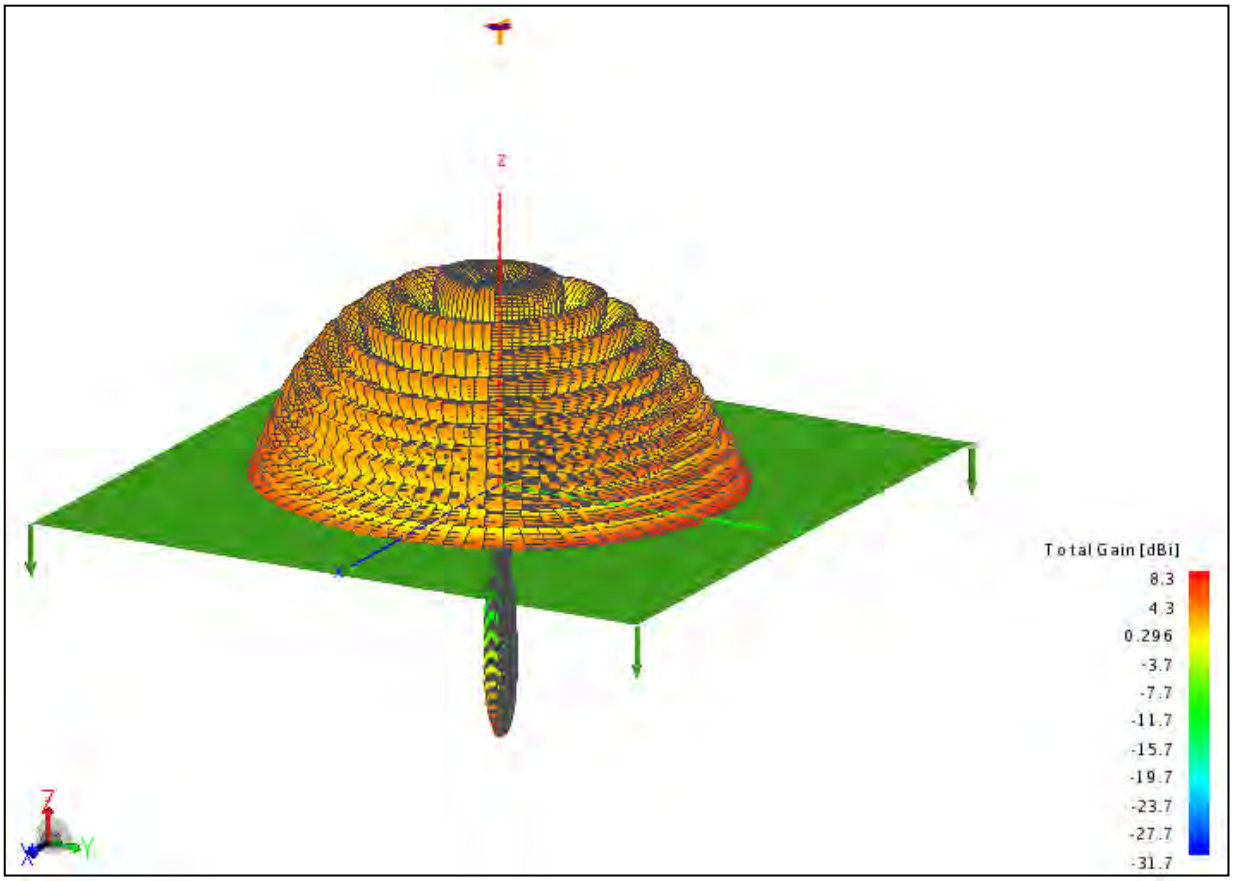

Figure 7. Gain pattern for the L antenna over real earth (green).

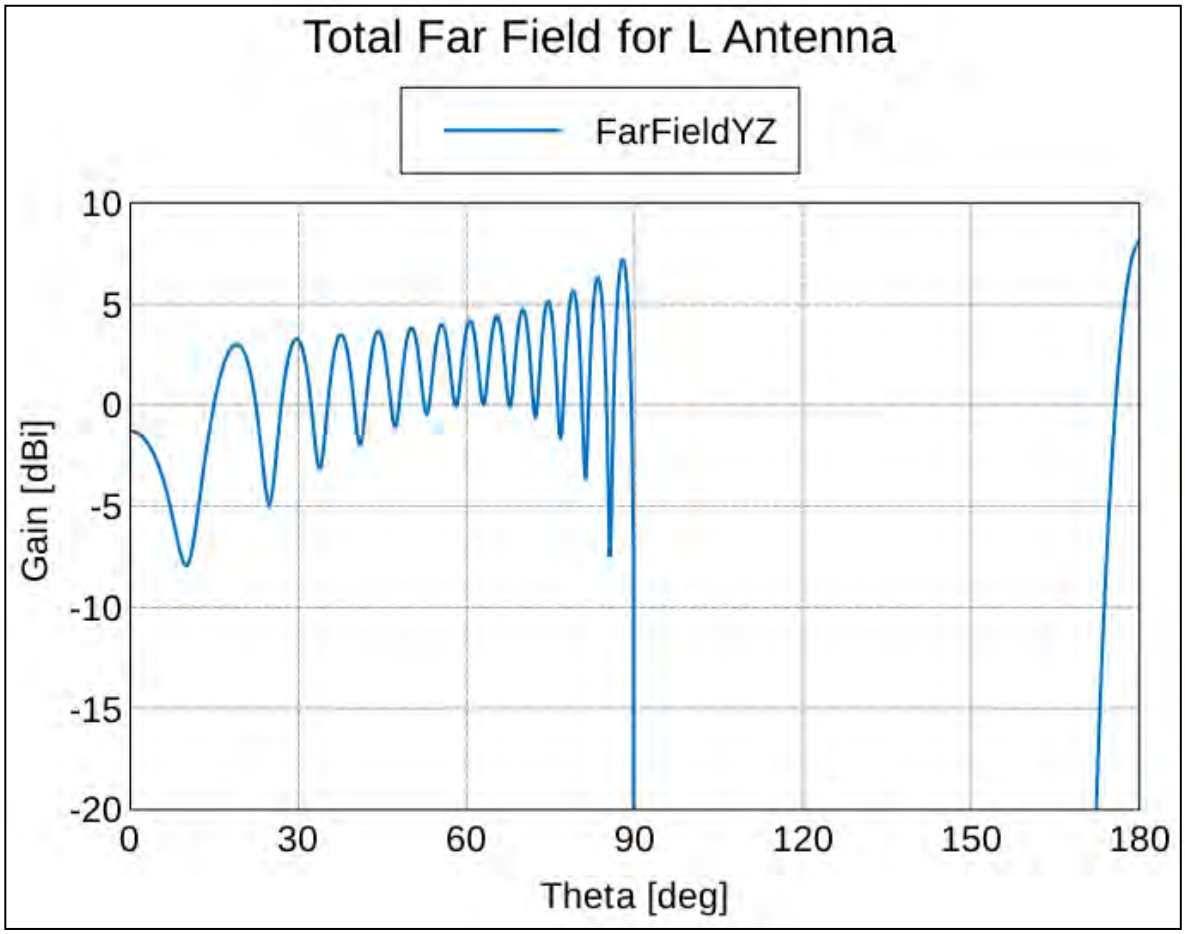

Figure 8. L antenna gain vs. θ in the plane orthogonal to the antenna plane (i.e., Y=0) over real earth (at 90°).

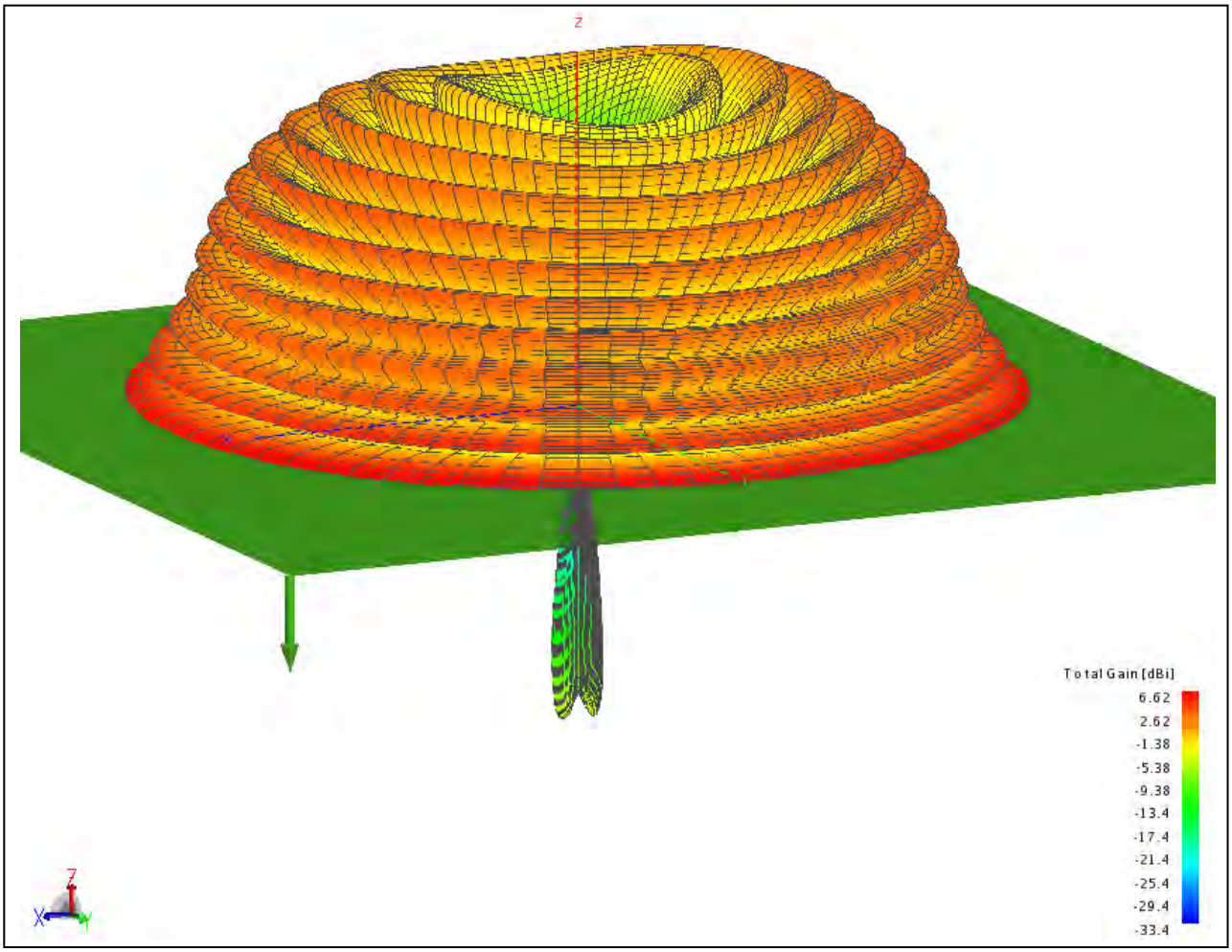

Figure 9. Gain pattern for the T antenna over real earth.

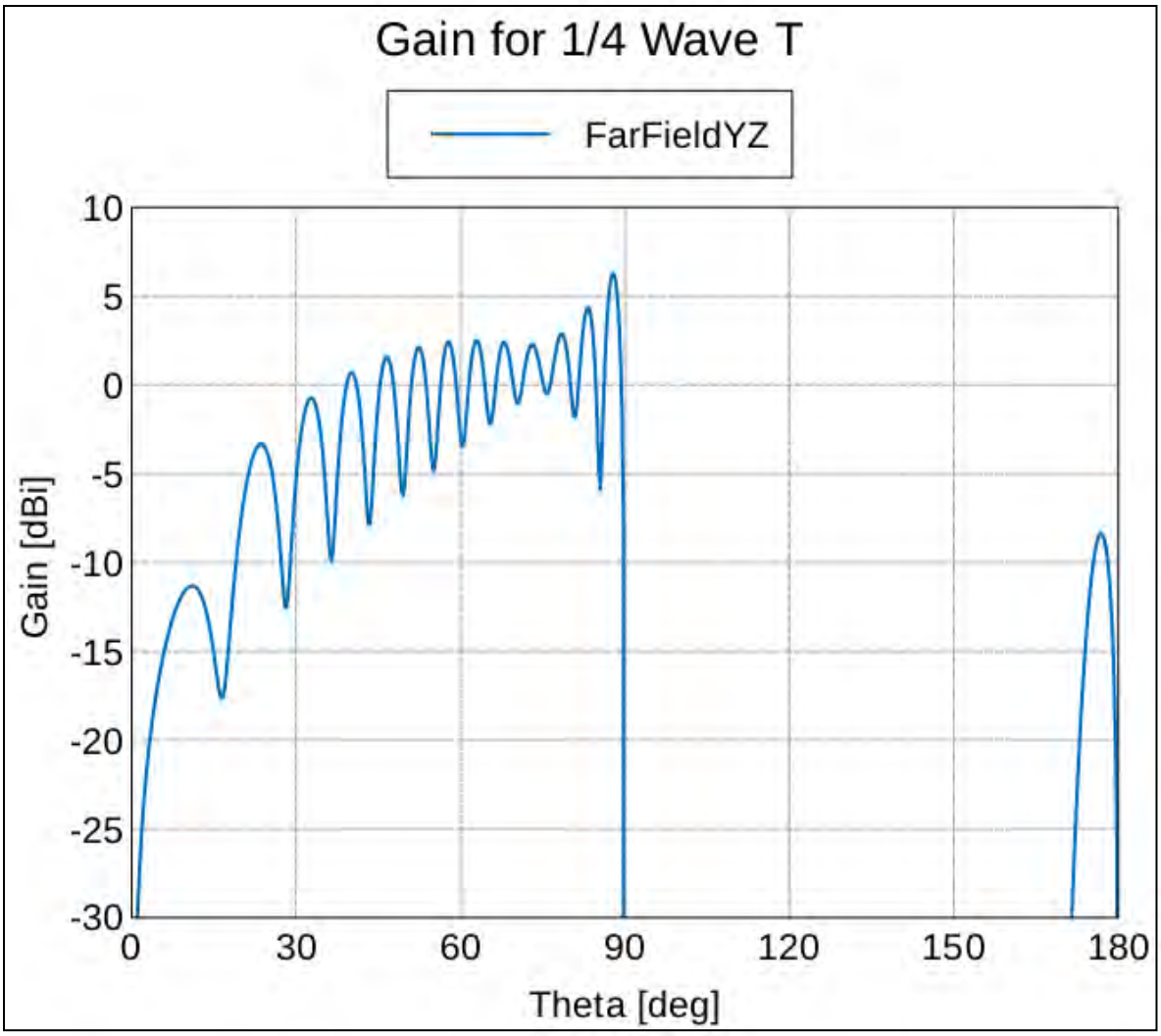

Figure 10. L antenna gain vs. θ in the plane orthogonal to the antenna plane (Y=0) over real earth (90°).

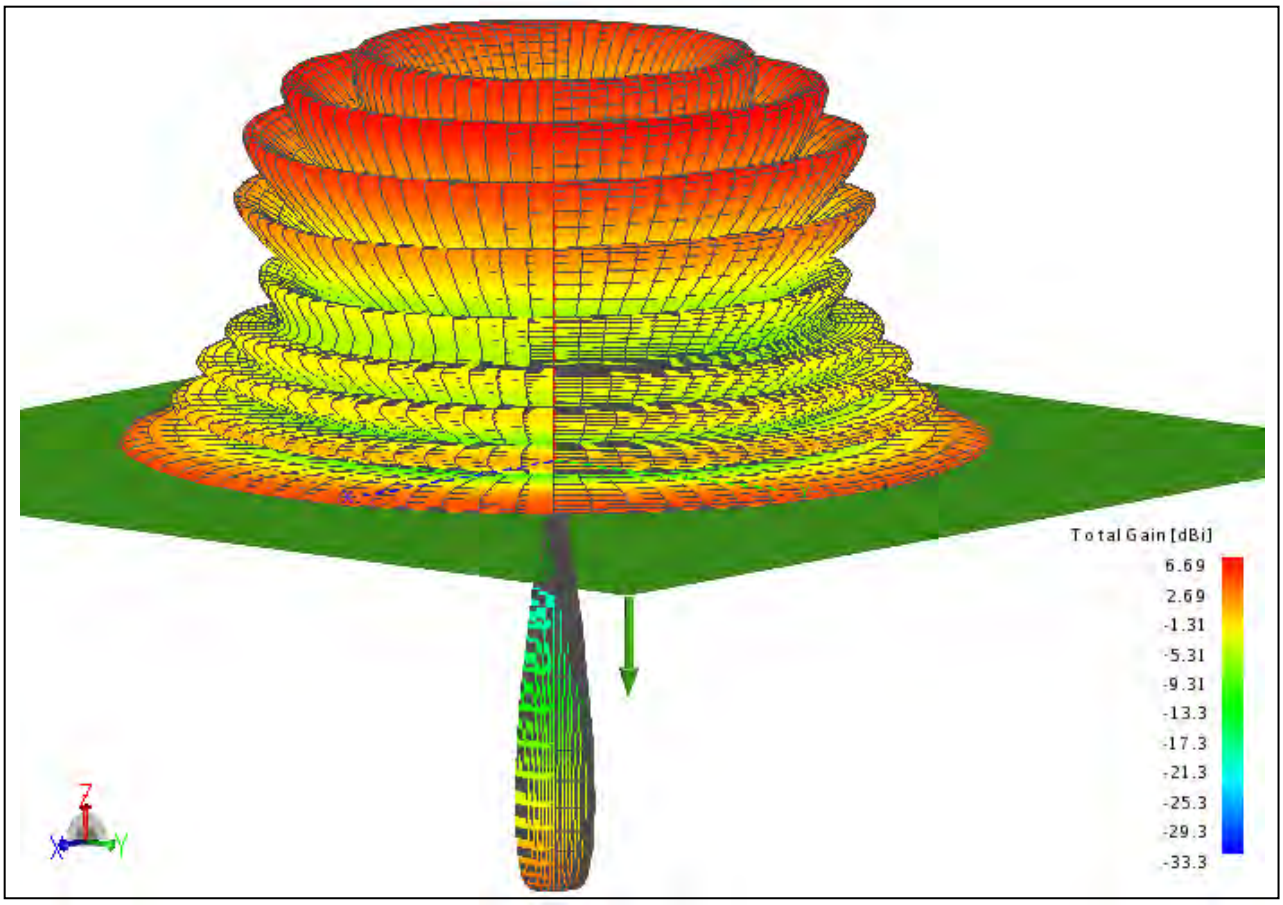

Figure 11. Gain pattern for the segmented antenna over real earth.

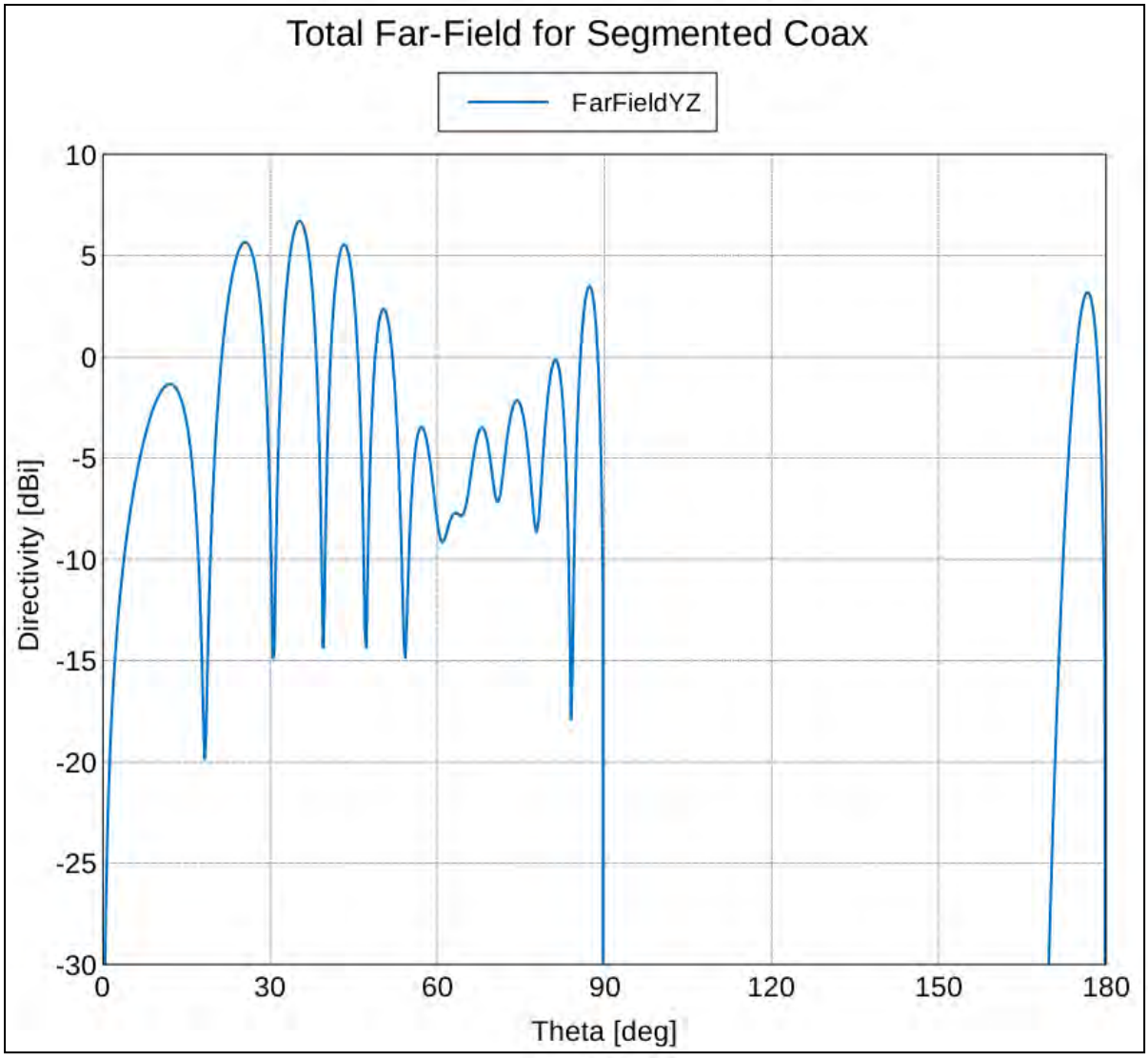

Figure 12. Segmented antenna gain vs. θ in the plane orthogonal to the antenna plane (Y=0) over real earth (90°).

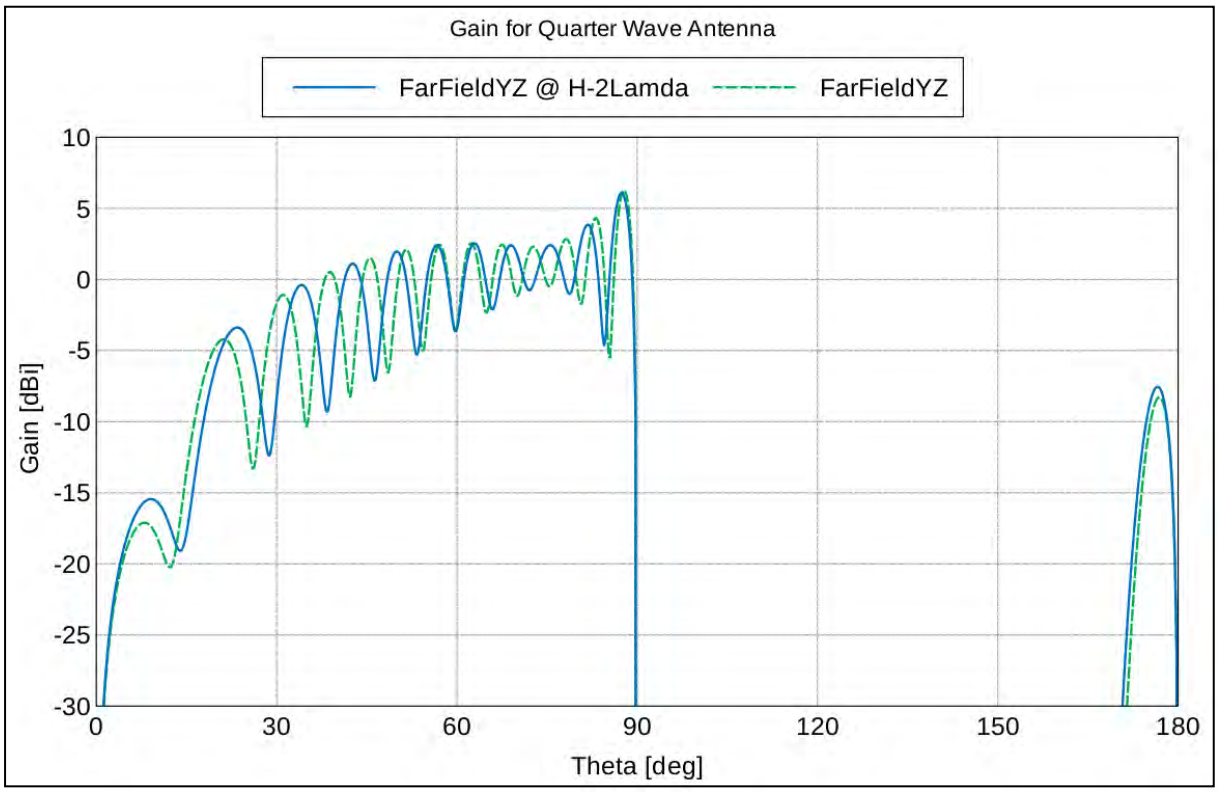

Figure 13. Gain for the T antenna at two elevations above ground. Lobe density increases with increasing elevation. The solid blue line corresponds to antenna elevation 2 λ lower.

3.2 Near Fields

We are interested in the fields from elevated antennas incident on the ground at large but finite distances. Far fields, for our purposes, are at infinite distances, but fields at the ground with a finite conductivity disappear at infinite distances. Therefore, we used "near field" computations to properly account for the fields on the ground at finite distances from the antenna, even though at 10 km the field is not "near field" in the conventional sense.

Figure 14 shows E_θ from the T antenna at points from 2° (or $\theta = 88°$) just above the ground down to the ground ($\theta = 90°$) at three different radii from beneath the antenna. The field near the ground is absorbed at greater distances. It rises up at 2° elevation consistent with the lobe near the ground shown in the far-field plots of figures 10 and 13. Fields above the ground are a sum of the direct and ground reflected waves of these two paths. The depth and position of the small dip in field strength within a tenth of a degree of ground is a function of the earth conductivity and dielectric constant. Varying these constants results in different phase shifts of the reflected wave, and therefore, a different total field at elevations above the ground.

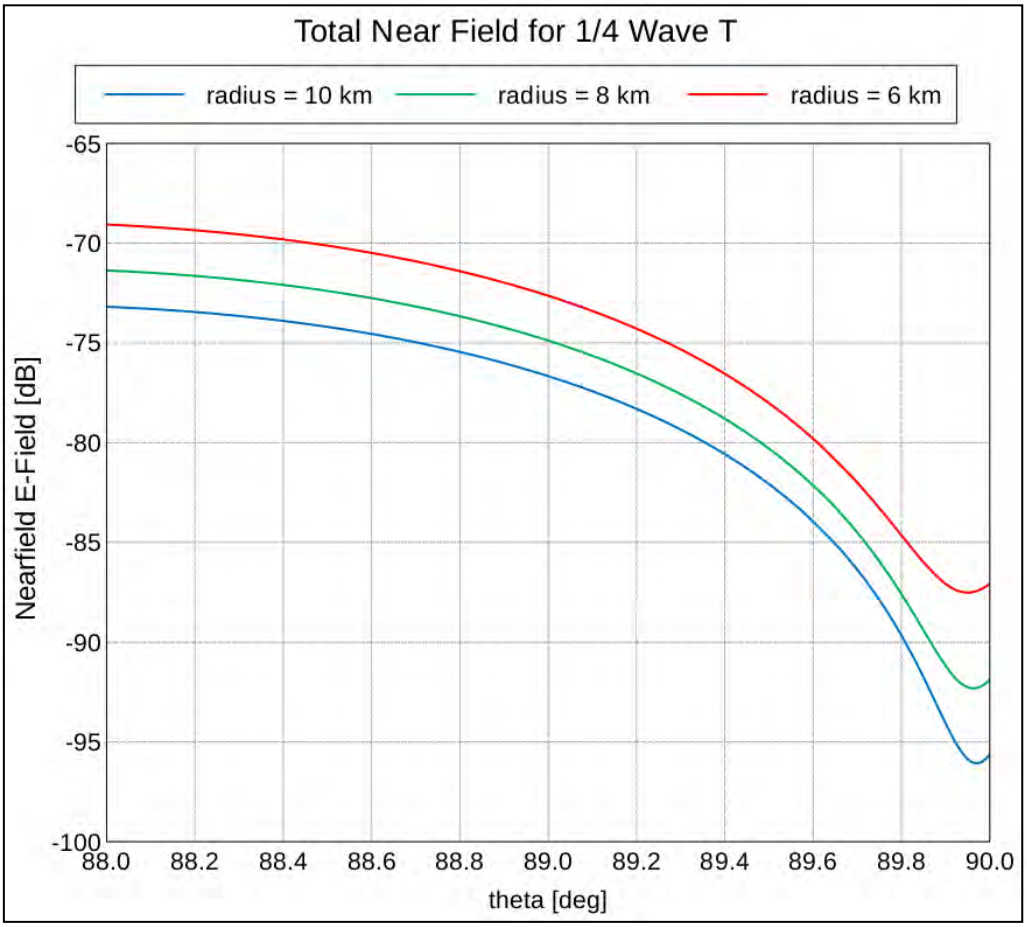

Figure 14. Computed total near field at and within 2° elevation above the ground for three distances from the antenna.

Figure 15 shows the field closest to the ground in more detail versus height in meters. The field does not change much, even if the target is located 2 m above ground.

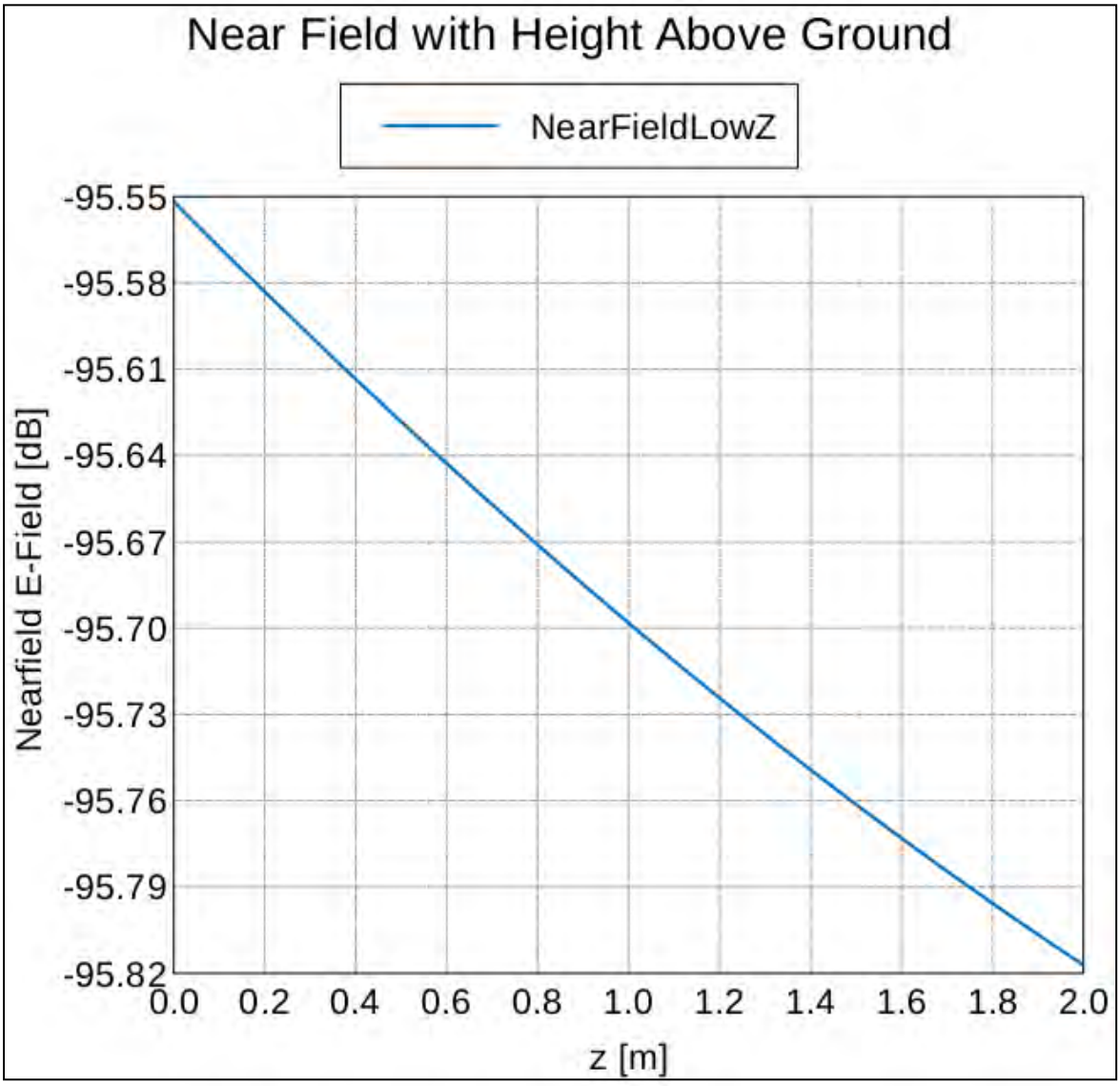

Figure 15. Closer look: Total near field at elevations at and near the ground in meters.

Figure 16 compares the field delivered to the ground by the three different antennas of this study. The T antenna clearly delivers the most field to the ground at 10 km and shorter distances from the antenna. It does so with a margin of about 6 dB at the highest distances over the L antenna and a margin of 9 to 10 dB over the segmented antenna at the distances of greatest interest.

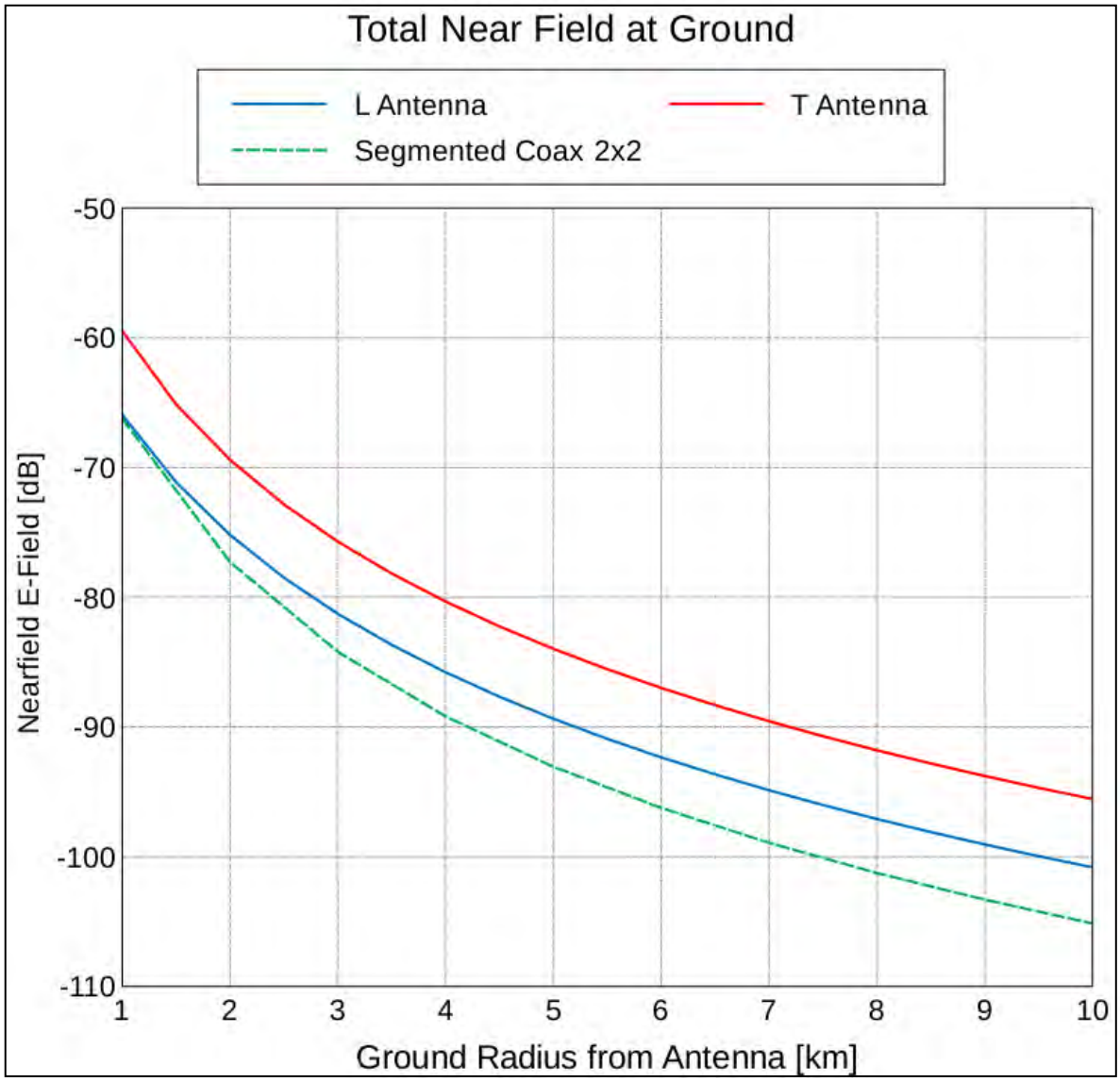

Figure 16. Ground near fields for the three antennas compared.

Figures 17 and 18 show features of the field behavior that could be of use in determining how high to set the antenna or of what use it might be for the intended application. The behavior exhibited in them is applicable to any of the antennas. This study focused on an antenna elevation of 4.4 wavelengths (λ). Figure 17 shows how the field strength delivered to the ground changes as the antenna is raised or lowered; doubling its elevation increases it by about 4 dB at 10 km out. Calculated using a plane wave approximation to the field at 10 km out figure 18 shows how the total field strength drops as it penetrates into the ground. Within a few centimeters, it drops by about 11 dB and after that it drops by about 2.5dB per meter of soil depth for our uniform soil.

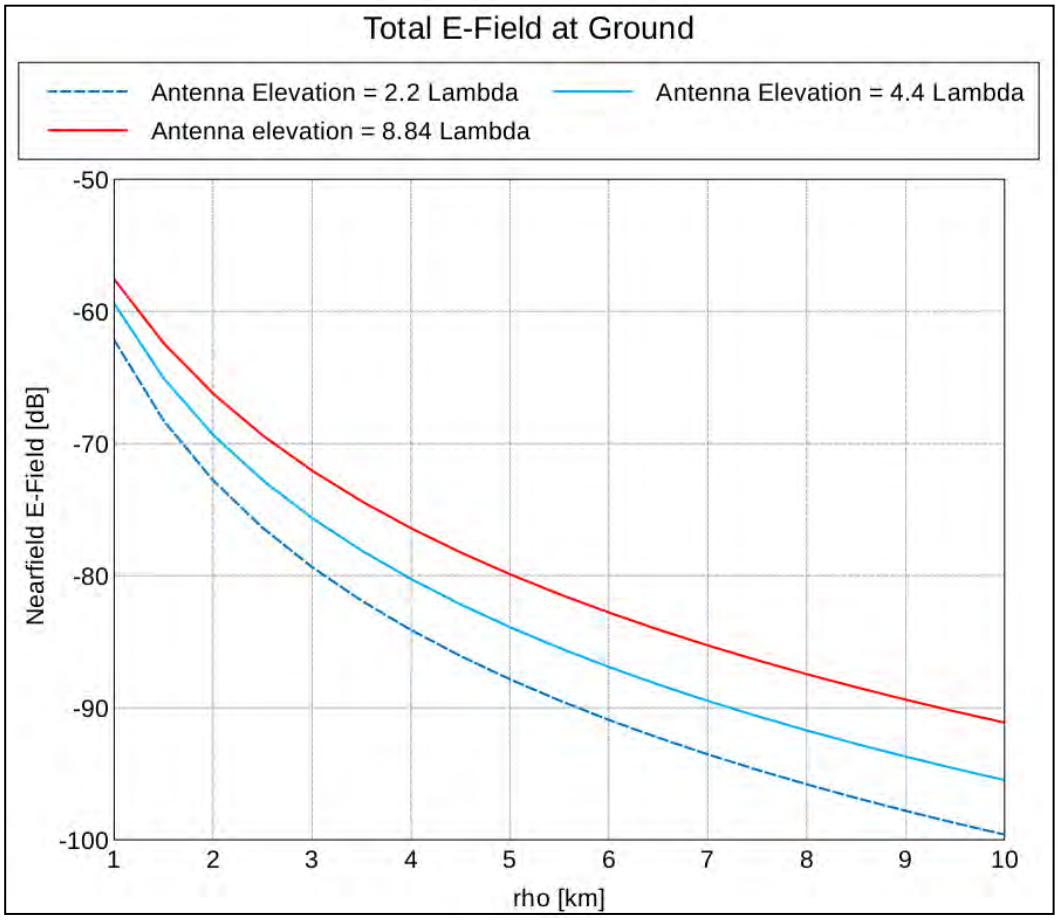

Figure 17. Total field at ground for three different antenna elevations vs. ground distance from the antenna.

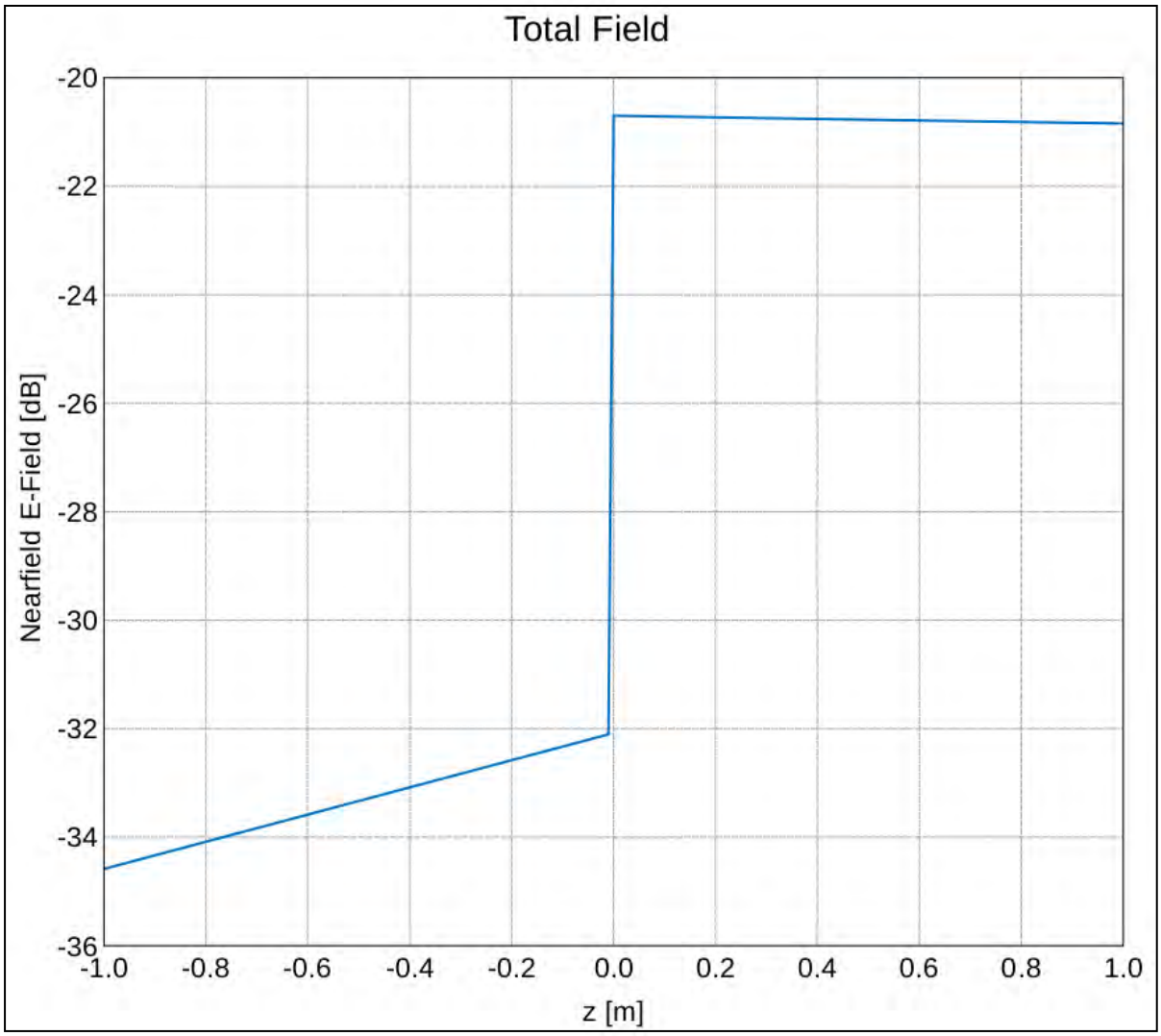

Figure 18. Plane wave penetration into ground for 10 km case.

4. Conclusions

In this study, the L antenna has a single ¼ wavelength counterpoise. If the ½ wavelength counterpoise of the T antenna is too long for the aerostat, then the L antenna might be preferred. Increasing the antenna elevation above ground would also deliver more energy to it.

The T antenna delivers the most energy at 10 km by 6 to 9 dB over the other antennas. It is also much lighter than the coaxial antenna and not much heavier than the L antenna. Therefore, it could be lifted to the necessary elevation by a medium size aerostat (~30 ft wide). We conclude that the T antenna is the preferred HF airborne candidate.

1 (PDF only) DEFENSE TECHNICAL INFORMATION CTR
DTIC OCA
8725 JOHN J KINGMAN RD
STE 0944
FORT BELVOIR VA 22060-6218

1 DIRECTOR
US ARMY RESEARCH LAB
IMNE ALC HRR
2800 POWDER MILL RD
ADELPHI MD 20783-1197

1 DIRECTOR
US ARMY RESEARCH LAB
RDRL CIO LL
2800 POWDER MILL RD
ADELPHI MD 20783-1197

1 DIRECTOR
US ARMY RESEARCH LAB
RDRL CIO MT
2800 POWDER MILL RD
ADELPHI MD 20783-1197

1 DIRECTOR
US ARMY RESEARCH LAB
RDRL D
2800 POWDER MILL RD
ADELPHI MD 20783-1197

21 US ARMY RSRCH LAB
ATTN RDRL SER M W COBURN
ATTN RDRL SER U T DOGARU
ATTN RDRL SER U C FAZI
ATTN RDRL SER U M HIGGINS
ATTN RDRL SER U K KAPPRA
ATTN RDRL SER U C KENYON (4 COPIES)
ATTN RDRL SER U C LE
ATTN RDRL SER U D LIAO
ATTN RDRL SER U A MARTONE
ATTN RDRL SER U G MAZZARO
ATTN RDRL SER U D MCNAMARA
ATTN RDRL SER U M RESSLER
ATTN RDRL SER U K SHERBONDY
ATTN RDRL SER U G SMITH
ATTN RDRL SER U B STANTON
ATTN RDRL SER U A SULLIVAN
ATTN RDRL SER U C TRAN
ATTN RDRL SER U D VANCE